Journal of Materials Science: Materials in Electronics (2020) 31:13011–13027
https://doi.org/10.1007/s10854-020-03930-6

REVIEW

A review on recent progress in rare earth and transition metals activated SrY_2O_4 phosphors

Ruby Priya[1] · Sandeep Kaur[1] · Utkarsh Sharma[1] · O. P. Pandey[1] · Sanjay J. Dhoble[2]

Received: 30 April 2020 / Accepted: 1 July 2020 / Published online: 15 July 2020

Abstract

SrY_2O_4 belongs to the family of AB_2O_4 (A = alkaline earth metal, B = rare earth element) type spinel oxides. SrY_2O_4 is an inter oxide in SrO and Y_2O_3 pseudo-binary phase diagram. It has attracted immense interest as a promising host lattice owing to its thermal and chemical stability. The luminescent characteristics of SrY_2O_4 phosphors make them promising candidates for field emission displays. In the present review article, recent progress in the synthesis and luminescent properties of bare and doped SrY_2O_4 phosphors are reviewed. In the first part, different synthesis routes and their resultant outcomes are discussed. Then, the downconversion and upconversion luminescent characteristics of undoped and doped SrY_2O_4 phosphors are reviewed. The effect of site occupancy, morphology, reaction conditions, different excitation wavelengths, dopant concentrations, and energy transfer mechanisms are explained in detail. In the end, challenges and future scope in luminescence and synthesis of SrY_2O_4 are proposed. This review article gives a complete summary for the drawbacks and current challenging issues of SrY_2O_4 phosphors, which can give potential sprout for future work.

1 Introduction

In the present era, field emission displays (FEDs) are in high demand due to their high brightness, less power consumption, low manufacturing cost, high contrast ratio, high efficiency, etc. [1–3]. To manufacture flat panel displays, phosphors play an important role. For this purpose, rare earth-doped inorganic materials have attracted much attention in the lighting industry. This is owing to the unique luminescent properties arising from the f–f orbital electronic transitions. In FEDs, the phosphors are operated at low excitation voltage (3–7 kV) and high current densities (10–100 μA cm^{-2}). Thus, the phosphors which can be efficiently operated at low voltages and resistant to current saturation with stable chemical and thermal properties are required. Till now, many commercial sulfide-based phosphors are used for commercial purposes such as ZnCdS:Ag:Cl, ZnCdS:Cu:Al, ZnS:Cu:Al, Y_2O_2S:Eu, Gd_2O_2S:Tb, and ZnS:Ag, Cl, $SrGa_2S_4$:Ce [4, 5]. However, these phosphors are not eco-friendly. They degrade under electron beam bombardment and release hazardous sulphur gas. Under electron bombardment, electrons cause the formation of oxides and sulphates which deposit on the screen of the device, also known as "dead layer". This decreases the lifetime of the device and restricts the use of sulfide-based phosphors in FEDs. Thus, potential phosphors are required, which are thermally stable and eco-friendly. For this purpose, oxide-based phosphors are considered as promising candidates due to their high physical, chemical, and thermal stability, low phonon energy, and high bandgaps, absence of blinking, gas free emission, and corrosion resistant properties.

Among the various rare earth oxides, binary rare earth oxides with structural composition ARE_2O_4 (A = Ca, Sr, Ba, Sr, RE = rare earth element) have become the topic of luminescent researchers. These have been studied by various researchers and are used in various lighting and display devices due to their unique optical, magnetic, and thermal properties [6–9]. Out of these inter oxides of alkaline earth metals and rare earth elements; SrY_2O_4 (SYO) has attracted research interest. It is an inter oxide in Y_2O_3–SrO pseudo-binary phase diagram. SYO possesses high physical, chemical, and thermal stability and also environment-friendly. Earlier, SYO due to its high thermal and chemical stability was

✉ O. P. Pandey
oppandey@thapar.edu

[1] Functional Materials Lab, School of Physics and Materials Science, Thapar Institute of Engineering & Technology, Patiala 147004, India

[2] Department of Physics, R.T.M. Nagpur University, Nagpur 440033, India

used in thermal barrier coatings and oxide fuel cells [10, 11]. The luminescent characteristics of SYO:Eu synthesized via combustion route were first reported by Park et al. [12]. Due to its high structural stability, it is considered a good host matrix for the doping of various elements. It is a suitable phosphor material for field emission displays (FEDs) owing to its emission properties and thermal stability. In addition, Ghorpade et al. [13] studied the photocatalytic activities of the Dy-activated SYO phosphors to degrade the Rohdamine-B dye. It was found that the efficiency of dye degradation decreased with doping. Moreover, due to the high bandgap around 4.9, it is not an efficient catalyst in comparison to the other existing semiconductor catalysts. However, 50% degradation of the dye was achieved. In another study, Dubey et al. [14] reported the thermoluminescent spectra of Eu-doped SYO. The phosphors were irradiated by radiations of 10 Gy Sr^{90} beta source. The samples showed second-order kinetics and corresponding trap depth was in between 0.18 and 0.5 eV. However, no other investigations using different irradiation sources, change of dopant concentrations, and variations in irradiation duration are reported. Thus, to use SYO phosphors for dosimetric applications, further investigations are required. The pictorial representation of various properties and applications of SYO is shown in Fig. 1.

In general, SYO is synthesized via high temperature ceramic route [15–17]. However, many researchers have attempted to synthesize it via soft chemical routes [18, 19]. Till now, many rare earth activators have been doped in the SYO host lattice and luminescent studies are conducted. The present review article is centered around the recent progress in the synthesis and luminescent properties of SYO phosphors.

The crystal structure of SYO is inverse spinel orthorhombic with Pnam group symmetry [20, 21]. The octahedral structure is composed of $[Y_2O_4]^{2-}$ framework with Sr^{2+} ions. In the SYO host lattice, there are two different sites for Y^{3+} ions, i.e., Y1 and Y2 with C_s group symmetry (shown in Fig. 2). In crystal lattice of SYO, atoms of O are placed at vertices and face-centerd sites of lattice, whereas Y1 is placed at almost octahedral void (body-centerd) and Y2 at the tetrahedral void. Both Y atoms are surrounded by six O-atoms [22]. Y2 atoms distort the environment due to the difference in ionic radius of O^{2-} and Y^{3+}. The Sr atoms are placed in octahedral voids (at edges), giving Cs symmetry [23, 24]. PL technique also predicted the presence of these sites in the SYO lattice. The site occupancy of different dopants at different sites and their emission behavior under different excitations led to different remarks on the various sites in SYO host lattice. These are all discussed in the PL section.

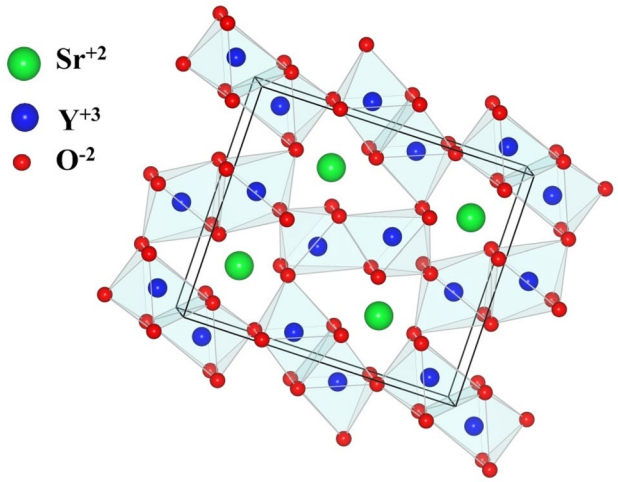

Fig. 2 Pictorial representation of SrY_2O_4 crystal structure

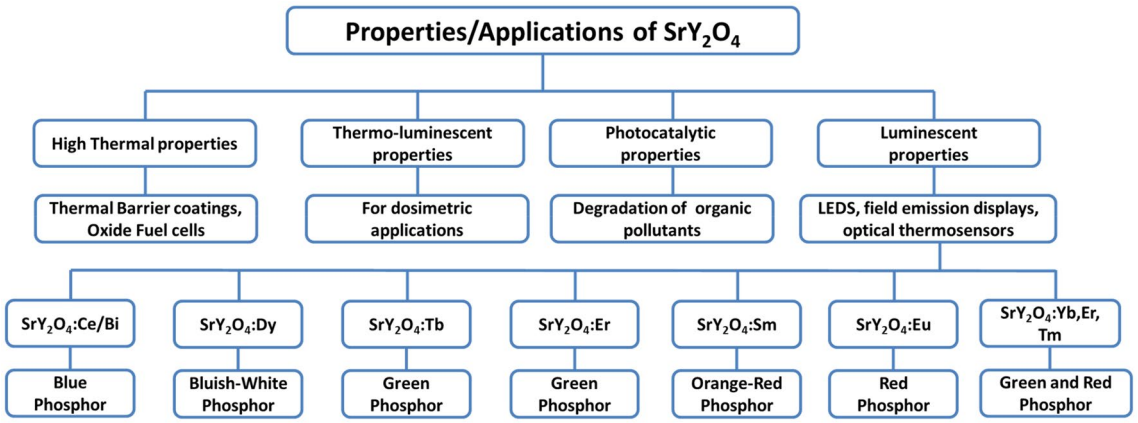

Fig. 1 Properties/Applications of SrY_2O_4 materials

2 Synthesis methods

Undoped and doped SYO phosphors are synthesized via adopting different synthesis routes. Till date, SYO materials are synthesized via solid-state, combustion, sol–gel, aldo–keto, and oil-emulsion methods. The detailed summary of precursors, additives, reaction conditions, and morphology are enlisted in Table 1. The details of synthesis routes are described and discussed in this section:

2.1 Combustion method

Combustion method is a constructive, convenient, eco-friendly, and efficient method for the synthesis of SYO compounds. This method requires the use of fuel such as urea, glycine, and sucrose to synthesize samples. The gases liberated during the burning of fuel generate high temperatures around 1500 to 1600 °C, which helps in the formation of phosphors at very low temperatures around 500 to 600 °C. SYO formed by the combustion route is synthesized using aqueous solution of metal nitrates as reducing agents and fuel as oxidizing agents, the amounts of which are calculated according to propellant chemistry. The aqueous solution is then placed in a preheated furnace at a lower temperature where voluminous ashes after completion of the combustion process are obtained. These ashes are further subjected to higher temperatures to obtain the pure phase, crystalline materials, and also to remove organic residues left behind.

Park et al. in 1999 synthesized Eu-doped SYO from metal nitrates in aqueous solution with urea as fuel. For Eu^{2+}-doped samples, the SYO was further subjected to successive heating ranging from 700 to 1000 °C in an H_2 stream [12]. Singh et al. in 2015 synthesized $SrY_2O_4{:}Eu^{3+}$ from metal nitrates and europium nitrate mixed with HMT as fuel. The solution was introduced in a preheated furnace at 600 °C and then further calcined at temperatures ranging from 800 to 1100 °C for 1 h [25]. Tamrakar and Upadhyay in 2017 synthesized SYO from metal nitrates using urea as a fuel. Then as-synthesized SYO was further annealed at 900 °C for 2 h to obtain pure phase [26]. Taikar in 2018 synthesized SYO from $SrCO_3$ and Y_2O_3 as precursors and adding NH_4NO_3 and urea as fuel. The mixture in the form of paste was put in a preheated furnace at 500 °C and was calcined at 1000 °C for 3 h to obtain pure phase phosphors [18]. Lojpur et al. in 2018 synthesized SYO from metal nitrates as precursors, citric acid, and glycine as fuel. The solution was prepared by mixing nitrates in deionized water, then citric was added and stirred for 30 min at 60 °C. Further glycine was added and stirred at 120 °C. Finally, the solution was burned in furnace at 500 °C for 1.5 h. Then, it was heated at 1000 °C for 2 h to obtain the phosphors [21]. The schematic presentation of combustion route is shown in Scheme 1.

2.2 Sol–gel method

Sol–gel method is an effective method to synthesize nanocrystalline SYO phosphors with uniform size distribution. In this method, metal nitrates of strontium and yttrium are dissolved with a chelating agent such as citric acid or oxalic acid**.** The solution is heated around 80–150 °C, which leads to the formation of xerogel. The xerogel is further heated to a specific temperature range to get pure phase SYO. The schematic presentation of the sol–gel method is shown in Scheme 2. Wang et al. in 2007 synthesized SYO from Y_2O_3 and $Sr(NO_3)_2$ as precursors and citric acid as a gelating agent via citrate-gel method. The gel was preheated for 2 h at 400 °C and then calcined at 1000 °C for 2 h [20]. Pavitra et al. synthesized Eu^{3+}/Dy^{3+} co-doped SYO, Eu^{3+}/Sm^{3+} co-doped SYO, Er^{3+} and Dy^{3+}/Sm^{3+} co-doped SYO phosphors using citrate sol–gel method. In their studies, they used citric acid to form a gel at 80 °C. The yellowish gel was further annealed at temperatures ranging from 700 to 1400 °C. However, pure phase SYO was obtained at 1300 °C. For temperatures, lower and above 1300 °C, Y_2O_3 was obtained as a secondary phase [15, 16, 27]. Zhang and Wang synthesized Eu-doped SYO phosphors via citrate sol–gel method. The xerogel formed was pre-fired at 600 °C for 4 h and further subjected at 1000 °C for 2 h in air [28]. Singh et al. in 2020 synthesized SYO by mixing metal nitrates and citric acid in aqueous solution. They used citric acid to form gel at 120 °C with 1 h stirring. The ratio of metal ions to citric acid was 1:2. Then, dried gel was heated in a furnace at 400 °C for 2 h. The obtained powder was annealed at 1000 °C for 3 h to obtain SYO phosphors [29].

2.3 Solid-state method

Solid-state method is an easy, adaptable, high temperature, and commonly used method to produce bulk SYO samples. This method leads to the formation of polycrystalline particles. The initial precursors are generally carbonates and oxides. In some cases, fluxing agents such as boric acid (H_3BO_3) in small quantities are used to lower the synthesis temperature. The schematic representation of solid-method is shown in Scheme 3.

Xu et al. in 2001 synthesized SYO by mixing strontium carbonate and yttrium oxide with boric acid as a chelating agent. These samples were pre-fired at 1000 °C for 2 h and then sintered at 1400 °C for 2 h [30]. Atkins et al. synthesized Eu^{3+}-doped SYO using Y_2O_3, $SrCO_3$ and Eu_2O_3 as precursors. The raw blend was ground and fired at 1050 °C for 18 h. It was again ground and fired at

Table 1 Synthesis conditions and outcomes of various methods

SrY_2O_4:dopant	Synthesis method	Precursors	Chelating agent (CA)/ gelating agent (GA)/fuel (F)/flux	Pre-firing temperature (duration)	Synthesis temperature (duration)	Morphology	Ref
SrY_2O_4:M (M = Eu^{3+}, Tb^{3+}, Sm^{3+}, Ce^{3+}, Bi^{3+})	Combustion synthesis method	$SrCO_3$, Y_2O_3	Urea (F)	–	1000 °C (PP) (3 h)	–	[18]
SrY_2O_4:Eu^{3+}	Combustion method	$Sr(NO_3)_2$,Y_2O_3, Eu_2O_3	Urea (F)	700 °C (6 h)	1000 °C (PP) (6 h)	–	[12]
MY_2O_4:Eu^{3+} (M = Mg, Ca, Sr)	Combustion method	$Y(NO_3)_3{\cdot}6H_2O$, $Eu(NO_3)_3{\cdot}6H_2O$, $Sr(NO_3)_2$	HMT (F)	–	1100 °C (PP) (1 h)	Spherical shape particles	[25]
SrY_2O_4:Tb^{3+}	Combustion method	$Sr(NO_3)_2$, $Y(NO_3)_3{\cdot}6H_2O$, $Tb(NO_3)_3{\cdot}5H_2O$	Urea (F)	–	900 °C (PP) (2 h)	Small agglomeration	[26]
SrY_2O_4:Eu^{3+}	Combustion method	$Y(NO_3)_3{\cdot}6H_2O$, $Eu(NO_3)_3{\cdot}6H_2O$, $Sr(NO_3)_2$	Glycine (F)	500 °C (1.5 h)	1000 °C (PP) (2 h)	Agglomerated particles	[21]
SrY_2O_4:Dy^{3+}	Combustion method	$Sr(NO_3)_2$, $Y(NO_3)_3{\cdot}6H_2O$, $Eu(NO_3)_3{\cdot}5H_2O$	Glycine (F)	–	1300 °C (3 h)	Nearly Spherical	[13]
SrY_2O_4:Eu^{3+}	Combustion method	$Sr(NO_3)_2$, $Y(NO_3)_3{\cdot}6H_2O$, $Eu(NO_3)_3{\cdot}5H_2O$	Glycine (F)	–	1300 °C (3 h)	Nearly spherical	[37]
SrY_2O_4:Eu^{3+}	Sol–gel method	$Sr(NO_3)_2$, $RE(NO_3)_3$ (RE = Y and Eu)	Citric acid (GA)	–	1000 °C (PP) (2 h)	Spherical-like shape	[38]
$Sr(Y,Gd)_2O_4$:Eu^{3+}	Sol–gel method	Y_2O_3, Gd_2O_3, $Sr(NO_3)_2$, Eu_2O_3	Citric acid (GA)	400 °C (2 h)	1000 °C (PP) (2 h)	–	[20]
SrY_2O_4:Tb^{3+}, Eu^{3+}, Sm^{3+}	Sol–gel method	$Y(NO_3)_3{\cdot}6H_2O$, $Sr(NO_3)_2$, $Eu(NO_3)_3$, $Sm(NO_3)_3{\cdot}6H_2O$, $Tb(NO_3)_3{\cdot}6H_2O$	Citric acid (GA)	400 °C (4 h)	700–1400 °C , 1300 °C (PP) (3 h)	Circular waves	[27]
SrY_2O_4:Eu^{3+}	Sol–gel method	$Sr(NO_3)_2$, $Y(NO_3)_3{\cdot}6H_2O$, $Eu(NO_3)_3{\cdot}6H_2O$	Citric acid (GA), glycine (F)	500 °C (1.5 h)	1000 °C (2 h)	Spherical-like	[39]
SrY_2O_4:Tb^{3+}, Tm^{3+}/ Dy^{3+}	Sol–gel Method	$Sr(NO_3)_2$, Y_2O_3, Dy_2O_3, Tm_2O_3, Tb_4O_7	Citric acid (GA)	500 °C (4 h)	1300 °C (3 h)	Aggregated crystallites	[17]
SrY_2O_4:Dy^{3+}, Eu^{3+}	Citrate sol–gel method	$Sr(NO_3)_2$, $Eu(NO_3)_3{\cdot}5H_2O$, $Y(NO_3)_3{\cdot}6H_2O$, $Dy(NO_3)_3{\cdot}5H_2O$	Citric acid (GA)	–	500 °C (PP) (5 h)	Closely packed with a single crystalline nature	[15]
SrY_2O_4:Er^{3+}, Sm^{3+}/ Dy^{3+}	Citrate sol–gel method	$Sr(NO_3)_2$, $Y(NO_3)_3{\cdot}6H_2O$, $Er(NO_3)_3{\cdot}5H_2O$, $Yd(NO_3)_3{\cdot}5H_2O$, $Sm(NO_3)_3{\cdot}6H_2O$	Citric acid (GA)	–	1300 °C (PP) (3 h)	Spherical shape	[16]
SrY_2O_4:Eu^{3+}	Sol–gel method	$Sr(NO_3)_2$, $Y(NO_3)_3$, $Eu(NO_3)_3$	Citric acid (GA)	600 °C (4 h)	1000 °C (PP) (2 h)	Highly aggregated	[28]
SrY_2O_4:Gd^{3+}	Sol–gel method	$Sr(NO_3)_2$, $Y(NO_3)_3{\cdot}6H_2O$, $Gd(NO_3)_3{\cdot}6H_2O$	Citric acid (GA)	400 °C (2 h)	1000 °C (PP) (3 h)	Aggregates of varying shape	[29]

Table 1 (continued)

SrY_2O_4:dopant	Synthesis method	Precursors	Chelating agent (CA)/ gelating agent (GA)/fuel (F)/flux	Pre-firing temperature (duration)	Synthesis temperature (duration)	Morphology	Ref
$SrY_2O_4:Ce^{3+}$	Solid-state method	$SrCO_3$, Y_2O_3, CeO_2	–	–	1200 °C (PP) (10 h)	–	[40]
$SrY_2O_4:Bi^{3+}$, Eu^{3+}	Solid-state method	$SrCO_3$, Bi_2O_3, Y_2O_3, Eu_2O_3	Ethanol (CA)	–	1400 °C (PP) (5 h)	–	[22, 34]
SrY_2O_4, $SrSm_2O_4$	Solid-state method	$SrCO_3$, Y_2O_3, Sm_2O_3	–	–	1650 °C (PP) (1 h)	Dodecahedral single crystals	[32]
SrY_2O_4	Solid-state method	$SrCO_3$, Y_2O_3	–	–	1500 °C (PP) (.05 h)	–	[11]
$SrY_2O_4:Eu^{3+}$	Solid-state method	$SrCO_3$, Y_2O_3, Eu_2O_3	–	600 °C (4 h)	1000 °C (PP) (2 h)	Highly aggregated	[28]
$SrY_2O_4:Eu^{3+}$	Solid-state method	$SrCO_3$, Y_2O_3, Eu_2O_3	Boric acid (flux)	1000 °C (2 h)	1400 °C (PP) (2 h)	–	[30]
$SrY_2O_4:Eu^{3+}$	Solid-state method	Y_2O_3, $SrCO_3$, Eu_2O_3	–	–	1050 °C (PP) (18 h)	–	[24]
$SrY_2O_4:Eu^{3+}$	Solid-state method	$SrCO_3$, Y_2O_3, Eu_2O_3	Boric acid (flux)	700 °C (2 h)	1400 °C (PP) (2.5 h)	–	[23, 31]
$SrY_2O_4:Eu^{3+}$	Solid-state method	$SrCO_3$, Y_2O_3, Eu_2O_3	H_3BO_3 (flux)	1000 °C (0.5 h)	1350 °C (PP) (3 h)	–	[14]
$SrY_2O_4:Er^{3+}$, Yb^{3+}	Solid-state method	$SrCO_3$, Y_2O_3, Er_2O_3, Yb_2O_3	NH_4Cl (flux)	–	1350 °C (PP) (3 h)	–	[33]
$SrR_2O_4:Eu^{3+}$ (R = Y,Lu)	Oil-emulsion method	$Sr(NO_3)_2$, $Y(NO_3)_3$, $Lu(NO_3)_3$, $Eu(NO_3)_3$	$H_2C_2O_2$ (CA)	–	800–1100 °C ; 1000 °C (PP) (2 h)	Rugby-like shape	[36]
$SrY_2O_4:Eu^{3+}$	Aldo–keto gel method	$Y(NO_3)_3$, $Sr(NO_3)_2$, Eu_2O_3	Acetone Benzaldehyde (GA)	–	1000 °C (PP)	Not uniform and having agglomeration	[35]
$SrY_2O_4:Eu^{3+}$	Polyol method	$Sr(NO_3)_2$, $Y(NO_3)_3{\cdot}6H_2O$, $Eu(NO_3)_3$	Urea (F)	–	1000 °C (PP) (5 h)	–	[41]

Here, PP denotes the temperature at which pure SYO phase was obtained. HMT denotes Hexamethylenetetramine

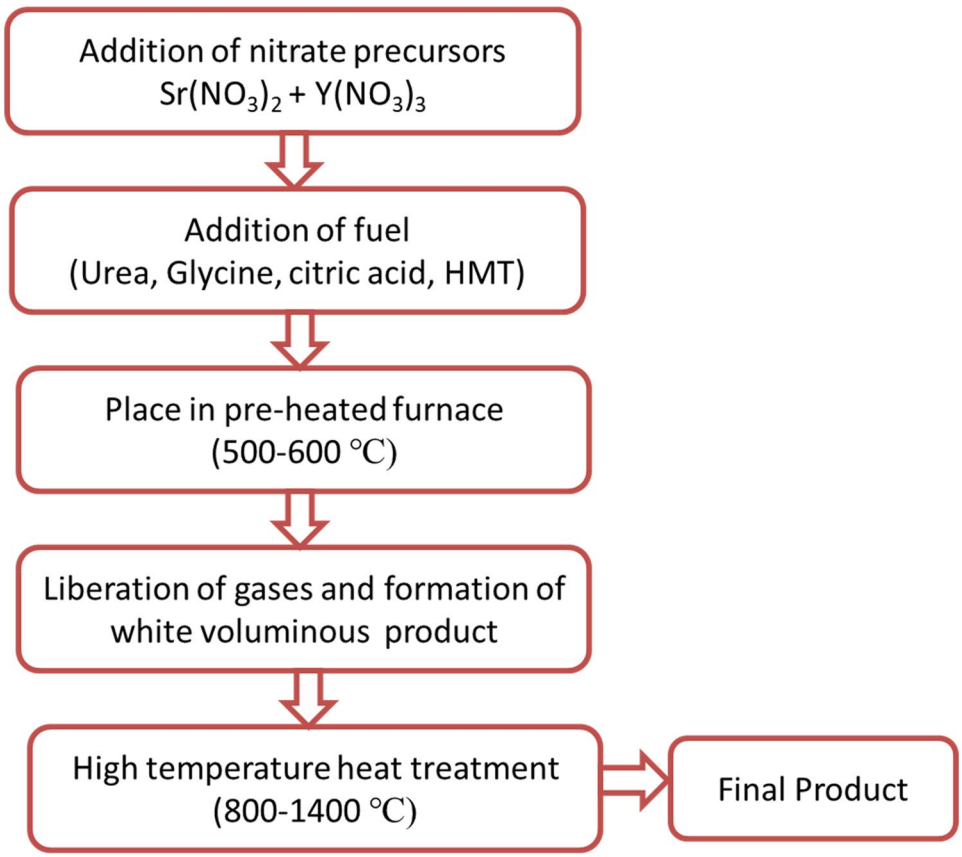

Scheme 1 Schematic representation of combustion route (based on the data collected from the literature)

1050 °C for 18 h to obtain SrY_2O_4: Eu^{3+} phosphors [24]. Fu et al. synthesized SYO by mixing strontium carbonate and yttrium oxide with 0.01 boric acid as flux. After thoroughly mixing, samples were heated at 700 °C for 2 h and then calcined at 1400 °C for 2.5 h in air [23, 31]. Zhang and Wang [28] and Dubey et al. in 2013 [14] synthesized SYO by thoroughly mixing of strontium carbonate and yttrium oxide. Firstly, the samples were subjected to 1000 °C in a furnace and then sintered at 1300 °C in air. The effect of Eu doping was studied in detail. Opravil et al. [32] synthesized SYO by homogenization of strontium carbonate and yttrium oxide via short milling for 10 min in vibration mill. The mixture was then treated in muffle kiln at 1650 °C for 1 h. The sintered pellet sample was next pulverized by grinding and fine milling to get the pure SYO phase. Xianlang et al. [33] synthesized Er^{3+}/Yb^{3+} co-doped SYO phosphors using $SrCO_3$ and Y_2CO_3 as initial precursors. NH_4Cl was used as a flux agent. The pure phase SYO phosphors were obtained after firing at 1350 °C for 3 h. Wei et al. [34] synthesized Bi^{3+}/Eu^{3+} co-doped SYO phosphors using $SrCO_3$ and Bi_2O_3 and Eu_2O_3 as initial precursors and ethanol as dispersing medium. The ground mixture was further annealed at 1400 °C for 5 h in air atmosphere. The crystallinity was obtained using 2 wt% H_3BO_3.

2.4 Other methods

Koparkar et al. [35] synthesized SYO by Aldo–keto method. This method consists of mixing of nitrates of strontium and yttrium in oxalic acid solution. Ethanol and benzaldehyde were added into the solution as gelating agents. Then, the pyrolysis of foam was observed at 450 °C. Further, it was burned at 1000 °C to obtain crystalline powder of SYO. In another study, Zhou et al. [36] synthesized SrR_2O_4:Eu^{3+} (R = Y,Lu) phosphors via water-in-oil microemulsion route. Two microemulsions (I and II) were prepared and mixed together with same phase. The microemulsion I consisted of $Sr(NO_3)_2$, $Y(NO_3)_3$/$Lu(NO_3)_3$ and $Eu(NO_3)_3$ solution while microemulsion II was 1.0 M $H_2C_2O_4$ solution which was used as a precipitating agent. The organic phase was composed of polyol ethylene octylphenol ether (OP-10), isopentanol, and cyclohexane in 2:1:6 volume ratio. The formed oxalate precursors were dried at 120 °C and annealed at different temperatures ranging from 800 to 1100 °C for 2 h. It was observed that temperature below 1000 °C consisted of Y_2O_3/Lu_2O_3, which were removed after annealing at temperature higher than 1000 °C.

From Table 1, it can be seen that the SYO phosphors were synthesized at higher temperatures. The morphology of the phosphors also plays a pivotal role in altering the

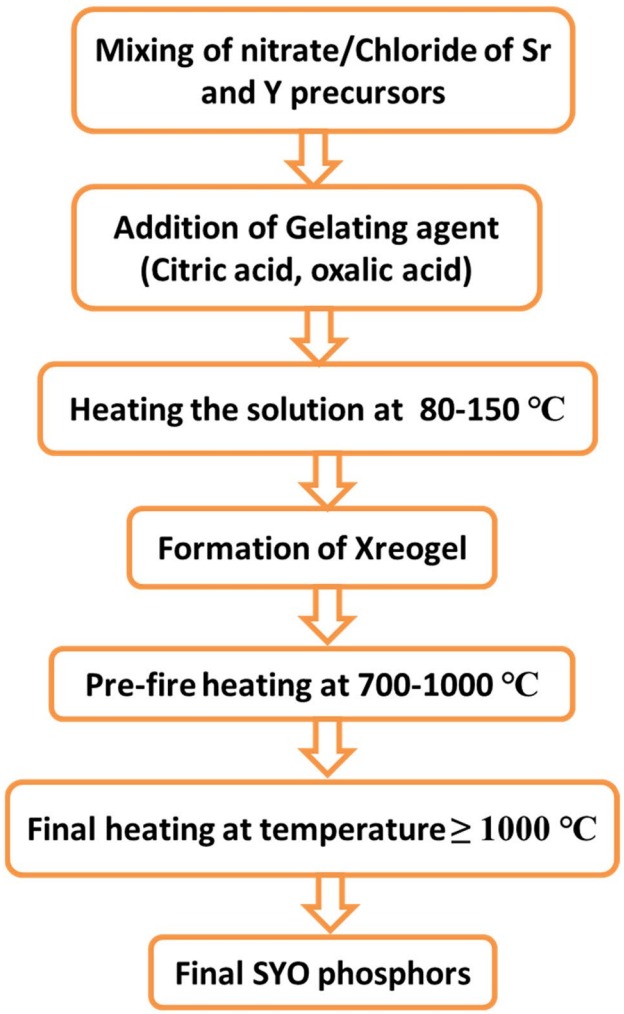

Scheme 2 Schematic representation of sol–gel method (based on the data collected from the literature)

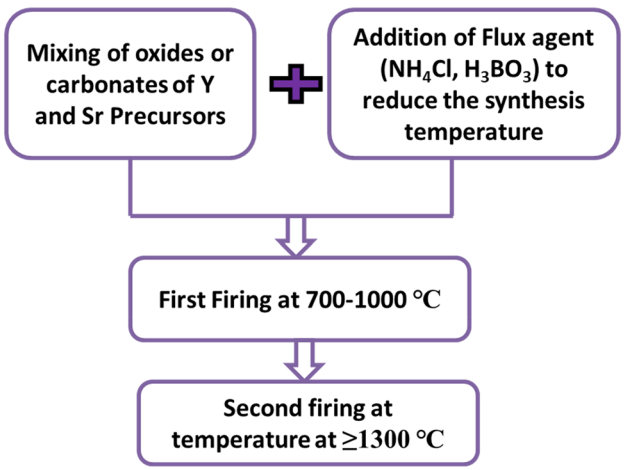

Scheme 3 Schematic representation of solid-state method route (based on the data collected from the literature)

luminescence properties. It can be observed from Table 1 that synthesized SYO phosphors via different routes exhibit different morphologies and particle size depending upon the precursors, reaction conditions, and use of additives. Singh et al. synthesized phosphors via combustion routes and observed narrow size distribution of spherical shape particles [25]. The particle size varied in the range of 10–25 nm. Lojpur et al. synthesized SYO:Eu via combustion route and found that particles were agglomerated having size ~ 50 nm with porous structures [21]. The porous features of the synthesized particles was attributed to the liberation of the gases during synthesis which ruptured the surface of the particles. Pavitra et al. synthesized SYO:Tb via sol–gel method and annealed at different temperatures [27]. It was observed that for pure phase SYO, the tip of every particle was in circular wave like shape, which might help to pack the particle closely. The closed packed particles are considered to prevent the scattering of light, which yields the light output efficiently. Moreover, it was observed that particle size increased gradually with the increase in the temperature. Pavitra et al. [16] synthesized SYO:Dy and found that particles exhibited uniform size spheres with close packing. Zhang and Wang [28] compared morphology of SYOEu synthesized via sol–gel and solid-state method. It was found that particles synthesized via solid-state method were agglomerated, whereas a better dispersion was obtained for samples synthesized via sol–gel method. Singh et al. [29] examined morphological features of SYO doped with Gd synthesized via sol–gel synthesis method. The particles were found to have aggregates of varying shape and size, which consisted of several small crystallites. These particles were highly interconnected having particle size ranging between 1 and 2 µm. Opravil et al. [16] observed the formation of dodecahedral single crystals and twin morphology of SYO:Sm synthesized via solid-state method. Zhou et al. [36] examined the morphology of SYO doped with Eu^{3+} synthesized by water-in-oil microemulsion and obtained rugby-like shape with diameter of 70–100 nm.

3 Photoluminescence (PL) in bare and doped SrY_2O_4 phosphors

SrY_2O_4 is a suitable host matrix due to its stable physical, chemical, and thermal structure [18]. It shows luminescent properties under UV and vacuum UV excitation. Zhang and Wang [28] synthesized undoped SrY_2O_4 phosphors by solid-state method. The excitation spectrum of SYO consisted of a band centered at 324 nm which was due to host absorption band. The band was appeared due to presence of defects which appeared due to preparation of samples at high temperature. It was further found that the antisite defects (Sr at Y site) could be considered to occur in the SrY_2O_4 structure,

and oxygen vacancies were also produced. Therefore, the excitation bands in the region of 290 to 360 nm when monitored at 406 nm, as well as the emission band around 406 nm excited at 324 nm, might have a relationship with defects in the SrY_2O_4 samples. So, the emission in SYO was considered due to presence of defects only. SYO itself is not a good luminescent material, however doping with different metal ions, it exhibits fascinating luminescent characteristics. In this section, downconversion and upconversion luminescent properties and various energy transfer mechanisms are discussed. The various photometric parameters of SYO phosphors are tabulated in Table 2.

3.1 Downconversion in SYO phosphors

When SYO is doped with Eu, Dy, Sm, Ce, Bi, and Tb, it exhibits downconversion spectra as shown in Fig. 3. The various factors affecting PL characteristics of doped SYO are discussed in this section.

3.1.1 SYO:Eu phosphors

Park et al. [12] prepared SrY_2O_4:Eu and $SrGd_2O_4$:Eu phosphors via combustion method. The excitation spectra of $SrY_{1.98}O_4$:$Eu_{0.02}$ were obtained at two different emission wavelengths, i.e., 611 nm (having maximum at 270 nm) and 616 nm (having maximum at 255 nm). The excitation bands were attributed to the charge-transfer transition within the [O^{2-}-Eu^{3+}] with diffused reflectance spectra. It was seen that the emission spectrum at 270 nm excitation mainly consisted of peaks corresponding to $^5D_0$–$^7F_0$, $^5D_0$–$^7F_1$, and $^5D_0$–$^7F_2$ transitions of Eu^{3+}. The presence of two resolved $^5D_0$–$^7F_=$ lines at 580.4 and 581.8 nm in the emission spectrum were believed to be due to the existence of at least two Eu^{3+} sites in the host lattice. Also, it was interesting to note that different excitation lines showed different emission spectra. The emission lines of two different excitation wavelengths (270 nm and 255 nm) were labeled as A (Eu^{3+} ion occupying the Y site) and B (Eu^{3+} ion to occupy the Sr site). It was

Table 2 Photometric parameters of SYO phosphors

Compound	Synthesis method	Excitation wavelength	Emission wavelength	Optimum concentration (mol%)	Lifetime	CIE coordinates	Ref
SrY_2O_4:Eu^{3+}	Combustion method	270 nm	616 nm	0.15	–	–	[12]
SrY_2O_4:Eu^{3+}	Microemulsion approach	272 nm	618 nm	9	2.25 ms	–	[36]
SrY_2O_4:Eu^{3+}	Sol–gel method	250 nm	609 nm	10	–	–	[17]
$SrY_{1.98}O_4$:0.02Eu^{3+}	Solid-state reaction	262 nm	616 nm	0.02	–	–	[28]
SrY_2O_4:Eu^{3+}	Sol–gel method	283 nm	616 nm	9	1.65 ms	(0.611, 0.366)	[27]
SrY_2O_4:Tb^{3+}	Sol–gel method	296 nm	543 nm	1	2.22 ms	(0.315, 0.508)	[27]
SrY_2O_4:Sm^{3+}	Sol–gel method	408 nm	608 nm	1	1.26 ms	(0602, 0.398)	[27]
SrY_2O_4:Eu^{3+}	Solid-state reaction	400 nm	613 nm	–	–	–	[35]
SrY_2O_4:Dy^{3+}	Citrate sol–gel method	351 nm	578 nm	1	–	(0.399, 0.400)	[15]
SrY_2O_4:Er^{3+}	Citrate sol–gel method	378 nm	548 nm	1	–	–	[16]
SrY_2O_4:Tb^{3+}	Solution combustion method	254 nm	–	2	–	(0.333, 0.391)	[26]
SYO:0.024Bi^{3+},0.09Eu^{3+}	Solid-state method	410 nm	611 nm	0.024(Bi), 0.09 (Eu)	–	(0.2281, 0.1157)	[34]
SrY_2O_4:Er^{3+}/Yb^{3+}	Solid-state method	1550 nm	552 nm	0.12 (Er), 0.08 (Yb)	–	–	[33]
SrY_2O_4:Eu^{3+}	Polyol method	255 nm	615 nm	3	–	–	[41]
SrY_2O_4:Eu^{3+}	Aldo–Keto method	272 nm	613 nm	0.02	–	(0.56, 0.35)	[35]
SrY_2O_4:Sm^{3+}	Combustion method	409 nm	610 nm	1	–	(0.586, 0.412)	[18]
SrY_2O_4:Ce^{3+}	Combustion method	345 nm	460 nm	1	–	(0.152, 0.206)	[18]
SrY_2O_4: Bi^{3+}	Combustion method	330 nm	420 nm	1	–	(0.158, 0.035)	[18]
$Sr(Gd,Y)_2O_4$	Citric–gel method	147 nm	611 nm	0.1	–	(0.647,0.352)	[20]
SrY_2O_4:Eu^{3+}	Combustion method	267 nm	612 nm	–	–	(0.5233, 0.3761)	[25]
SrY_2O_4:Er^{3+}	Co-precipitation method	980 nm	551 nm	0.5	–	(0.23, 0.73)	[44]
SrY_2O_4:Eu^{3+}	Citrate sol–gel method	393 nm	611 nm	5	45 µs	–	[39]
SrY_2O_4:0.005Tm:0.003Dy	Pechini sol–gel method	217 nm	455 nm	0.005 (Tm), 0.003 (Dy)	–	(0.315, 0.333)	[17]
SrY_2O_4:1Er:1Tm:3Yb	Citrate sol–gel method	980 nm	551 nm	1 (Er), 1 (Tm), 3 (Yb)	–	(0.314, 0.34)	[45]
SrY_2O_4:Eu^{3+}	Combustion method	280 nm	614 nm	8	–	–	[21]
SrY_2O_4:Dy^{3+}	Combustion method	354 nm	581 nm	3	–	(0.261, 0.276)	[13]
SrY_2O_4:Eu^{3+}	Combustion method	254 nm	613 nm	11	–	(0.561, 0.421)	[37]

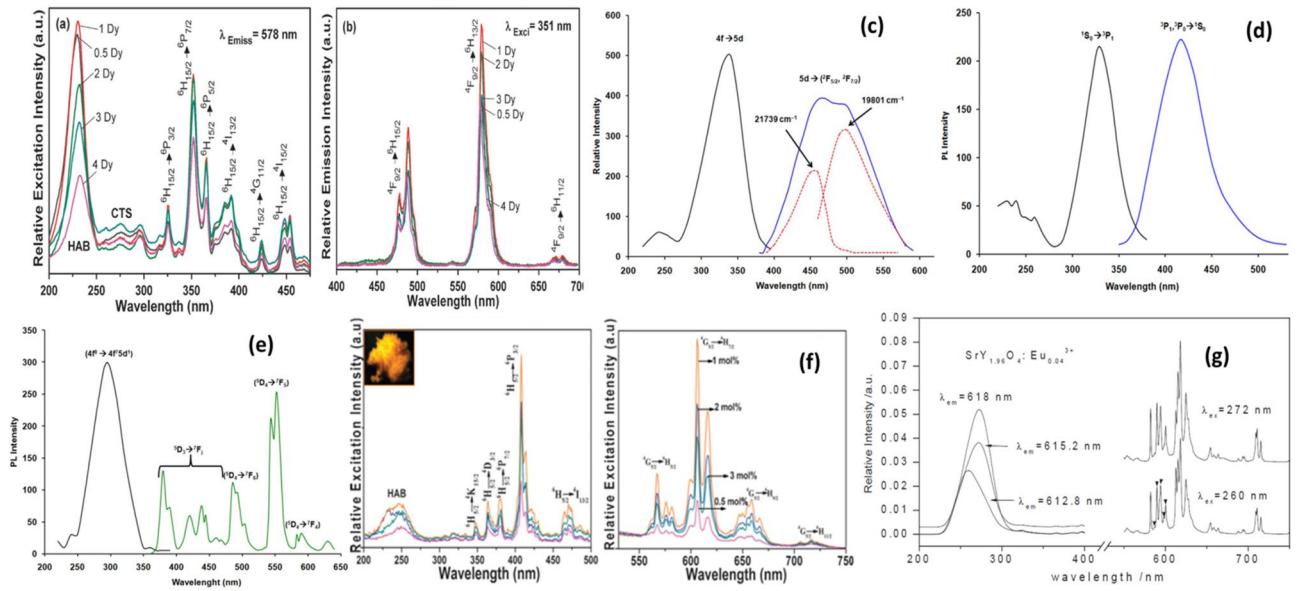

Fig. 3 **a**, **b** PLE and PL spectra of SYO:Dy [15], **c** PLE and spectra of SYO:Ce [18], **d** PLE and PL spectra of SYO:Bi [18], **e** PLE and PL spectra of SYO:Tb [18], **f** PLE and PL spectra of SYO:Sm [27] and **g** PLE and PL spectra of SYO:Eu [36] (with permission)

noticed that the emission intensities of site B were relatively increasing more rapidly than the site A as the concentration of Eu^{3+} was increased. It was suggested that Eu^{3+} ions in SYO occupied one Sr and two Y sites. At lower concentration ($x = 0.0025$), A site emissions dominated, whereas at higher Eu^{3+} ($x = 0.15$) concentration as the environment of two Y sites was changed the emission intensity of site B dominated. It was worth noting that apart from charge-transfer bands, each excitation spectra also consisted of an additional excitation band around 295 nm. The emission studies of the same samples showed a broad band emission around 470 nm in addition to Eu^{3+} emission lines which was too broad for emission from divalent Eu^{2+} emission. The studies of undoped SrY_2O_4 (reduced in the H_2 stream) showed the blue emission could be due to some crystal defects introduced by the reduction, not to the divalent Eu^{2+}. Further analysis showed that in the excitation spectra obtained by monitoring the B site emissions, the intensity of the defect band was comparable to that of the charge-transfer band. It was concluded that the energy transfer from the defect to Eu^{3+} ion in the B site might be more effective than that in the A site.

In another study, Zhou et al. [36] prepared $SrR_2O_4:Eu^{3+}$ (R = Y, Lu) superfine phosphors with rugby-like shape by microemulsion approach. Upon exciting the samples at different exciting wavelength from 257 to 272 nm, $SrY_{1.96}O_4:Eu^{3+}{}_{0.04}$ showed strong emission at 595.2 nm and 618 nm, due to f-f transitions of Eu^{3+}. It was worth noting that the purely magnetic transition appeared as five lines which were because of two sites of Eu^{3+} ions. By considering the different valence states and different ionic sizes of Sr^{2+} (113 pm) and Eu^{3+} (95 pm), as the calcination temperature was not high enough for Eu^{3+} to substitute Sr^{2+}, and the replacement of Eu^{3+} to Y^{3+} (89 pm) happened. Hence, two sites of Y^{3+} ions with the similar dimension of O^{2-} polyhedron in SrY_2O_4 lattice, led to the charge transfer from the oxygen ions to the substituting Eu^{3+}. A similar splitting for the transition $^5D_0$ to $^7F_2$ was also observed. The excitation studies on $SrLu_{1.96}O_4:Eu^{3+}{}_{0.04}$ at 613 nm, 615 nm and 618.6 nm, respectively, gave the excitation bands at 257 and 269 nm. Upon excitation with 257 nm and 269 nm, five $^5D_0$ to $^7F_1$ transition peaks also indicated that the Eu^{3+} ions occupied two non-equivalent Lu^{3+} ion sites. The highest intensity of $SrY_2O_4:Eu^{3+}$ and $SrLu_2O_4:Eu^{3+}$ was found at doped Eu^{3+} concentration of about 9 mol% and 6 mol%, respectively. Higher Eu^{3+} beyond the optimum concentration of Eu ions led to PL quenching.

Atkins et al. [24] studied the spectroscopic properties of Eu^{3+}-doped SrY_2O_4 under UV and VUV (vacuum ultraviolet) excitation. It was observed that peaks at 609 and 615 nm were sensitive to the excitation wavelengths. An opposite trend in peak intensity at 609 nm was observed under charge-transfer excitation at 250 nm and host lattice excitation at 150 nm. At 250 nm excitation, the intensity of the 609 nm emission line increased as Eu^{3+} content was increased, whereas it decreased for 150 nm excitation. These optical results again suggested the presence of two emission centers corresponding to the two Y sites in the host. By using host to activator energy transfer approach, they calculated that energy transfer was slightly more efficient to Y(2)

site. It was also found that the 35% of the excitation energy was lost to the surface states. Zhang et al. [28] compared the PL properties of $SrY_{1.98}O_4$:0.02Eu^{3+} prepared via solid-state and sol–gel method. It was found that the excitation spectra (at 616 nm) consisted of two bands (242 and 262 nm) when Gaussian deconvoluted. The band at 242 nm was attributed to the charge-transfer band (CTB) of Eu^{3+} ions occupying Sr^{2+} sites and the peak at 265 nm to the Eu^{3+} occupying two Y sites. It was interesting to observe that only one band was found for 610 nm, which suggested that this band was due to the Eu^{3+} ions occupying Sr^{2+} sites. The excitation spectra of the samples derived through sol–gel and solid-state methods exhibited the same trend, except the bands at 324 and 406 nm were disappeared in case of sol–gel method due to the absence of defects produced at high temperature. The emission spectra at 324 nm excitation showed that the emission intensity increased with increase in the Eu^{3+} concentration but the intensity of band at 406 nm decreased. This was due to the energy transfer from the defects to the Eu^{3+} ions at Sr^{2+} ions. The phosphors were excited at vacuum UV excitation (147 nm). Both the sol–gel and solid-state method derived samples which exhibited the same emission spectra. However, higher PL emission was obtained for samples prepared by sol–gel method when compared to samples prepared by solid-state reaction. It was because the surface quality of the phosphor particles that plays a vital role in luminescence efficiency. The samples prepared by sol–gel method seemed to have uniform dispersion of particles. Hence, it demonstrated that morphology characteristics also influenced the PL properties to a great extent. But unlike in the UV region, the spectra in VUV region did not show much difference except for the luminescence intensity for phosphors prepared by solid-state reaction and sol–gel method.

In another study, Pavitra et al. [27] studied the luminescent properties of SrY_2O_4 (SYO):Eu^{3+} phosphors synthesized via sol–gel method. The photoluminescence excitation (PLE) spectra of the SYO:Eu^{3+} phosphors at different Eu^{3+} concentrations at the emission wavelength of 616 nm revealed the broad excitation band, also called charge-transfer band (CTB) and the sharp excitation peaks due to f–f transitions of Eu^{3+} ions. It was found that the CTB position shifted towards the lower energy side (higher wavelength) with increasing annealing temperature, indicating the decreased quantum efficiency of Eu^{3+} ions. This redshift was explained on the fact that electrons in O^{2-} ions were less stable for the nano-scale particles and the surface to volume ratio was high as compared to the bulk sample; this increased the degree of disorder of the nanostructured system. Therefore, it required less energy to remove an electron from an O^{2-} ion; as a result, the CTB shifted towards the lower energy side. The PL spectra showed that phosphors exhibited emission bands ascribed to transition of the Eu^{3+} ions. The maximum PL intensity was observed at 9 mol%, and above this concentration quenching followed. Koparkar et al. [35] synthesized SrY_2O_4:Eu^{3+} phosphors via aldo–keto gel method. The excitation spectra consisted of a broadband widening from 200 to 310 nm region of UV radiation attributed to the charge-transfer band of O^{2-} to Eu^{3+} and some sharp lines at near UV–Visible region. The emission spectra showed a number of peaks in the range 500 to 700 nm corresponding to $^5D_0$–$^7F_{J\ (J=1,\ 2\ and\ 3)}$ transitions of Eu^{3+} monitored at 272 nm. The concentration of Eu^{3+} ion was varied in $SrY_{2(1-x)}O_4$:xEu (x = 0.001, 0.002, 0.005, 0.01, and 0.02). It was found that the emission intensity increased with the increase in Eu^{3+} concentration. It was ascribed to the fact that dopant did not alter its position in the lattices with increase in concentration. Also, the dipole moments of the Eu^{3+} were not affected by the increasing concentration.

Xu et al. [30] prepared both polycrystals and single crystals SrY_2O_4:0.01Eu^{3+} phosphors. Polycrystals were prepared by combustion method, while single-crystal fibers were grown in the air by the laser-heated pedestal growth (LHPG) method. The emission spectra of SrY_2O_4:0.01Eu^{3+} was recorded under two different excitations at 250 and 270 nm. It was found that under excitation at 270 nm, the emission peak intensity at 579.3 nm was comparable to the peaks near 616 nm, whereas under the excitation at 250 nm, the intensity was 20 times stronger than the peak at 581 nm. The authors extended their studies to SrY_2O_4:0.01Eu^{3+} single-crystal fibers to clarify the site occupation of Eu^{3+} doped in SrY_2O_4. The emission spectra were recorded under different excitation wavelengths at 240, 270, and 320 nm. It was observed that under excitation at 320 nm, peak at 578.1 nm was observed corresponding to $^5D_0$ to $^7F_0$ transition. It was concluded from the SrY_2O_4:Eu^{3+} single crystals that emission occurred from the three sites of Eu^{3+} ions; one at Sr^{2+} site and two at Y^{3+} sites, respectively. Wang et al. [20] prepared Eu^{3+}-doped $Sr(Gd,Y)_2O_4$ powder samples via citric-gel method. It was found that the excitation spectra of $SrY_{1.9}Eu_{0.1}O_4$ and $SrY_{1.0}G\ d_{0.9}Eu_{0.1}O_4$ were identical. The excitation bands around 149 and 204 nm were assigned to the host absorption, which was most likely to originate from the related charge-transfer band (CTB) of O^{2-}–Y^{3+}, as these became very weak in $SrGd_{1.9}Eu_{0.1}O_4$. Other two bands were observed in the UV range with peaks at about 230 and 275 nm attributed to the charge-transfer transition from two different Eu sites in SrY_2O_4:Eu^{3+}. The emission spectra of $SrY_xGd_{1.9-x}Eu_{0.1}O_4$ was recorded at 147 nm excitation and three samples ($SrY_{1.9}Eu_{0.1}O_4$, $SrY_{1.0}Gd_{0.9}Eu_{0.1}O_4$, and $SrGd_{1.9}Eu_{0.1}O_4$,) had similar emission spectra except intensity. The emission spectra of $SrY_xGd_{1.9-x}Eu_{0.1}O_4$ were composed of groups of several sharp lines corresponding to the transitions of Eu^{3+} ions. The calculated CIE coordinates for $SrY_xGd_{1.9-x}Eu_{0.1}O_4$ at 147 nm were in red region. It was noticed that $SrY_{1.9}Eu_{0.1}O_4$ had the highest emission

intensity. This implied that the Eu^{3+} emission was not efficiently sensitized by Gd^{3+}, which might be due to the narrow host bandgap and no efficient energy transfer occurred in the VUV region.

Fu et al. [31] compared the PL properties of blue and nanocrystalline SrY_2O_4:Eu phosphors. SrY_2O_4:Eu^{3+} nanocrystals were synthesized by PVA + glycine-assisted combustion method, whereas bulk SrY_2O_4:Eu^{3+} crystals were prepared by the solid-state method. It was observed that different excitation spectra were obtained at 611 and 616 nm for bulk SrY_2O_4:Eu^{3+}. The excitation bands were ascribed to the CT from the 2p orbital of O^{2-} to the 4f orbital of Eu^{3+} observed at 248, 257, and 270 nm. The CT bands in the SrY_2O^4:Eu^{3+} nanocrystals shifted to higher energies compared with those in bulk material. It was found that upon UV excitation, emission spectra exhibited characteristic peaks of Eu ions and also emission lines from higher ^5D levels were also observed. It was found that in case of bulk SrY_2O_4:Eu^{3+}, Eu^{3+} ions occupied three non-equivalent sites: one at the Sr site, two at Y(1) site and Y(2) site, while in nanocrystalline SrY_2O_4:Eu^{3+}, the Eu^{3+} ions occupied only two non-equivalent sites, i.e., Y(1) and Y(2) site.

Singh et al. [25] prepared a series of red–orange light-emitting phosphors, MY_2O_4 (M = Mg, Ca, and Sr) doped with Eu^{3+} via combustion process using hexamethylenetetramine as an organic fuel and done calcination at 800 and 1100 °C. The excitation spectra for all the phosphors at 612 nm emission wavelength consisted of broad bands due to f-f transitions of Eu^{3+} ion. It was found that the emission intensity of SrY_2O_4:Eu^{3+} nanophosphor was maximum, while MgY_2O_4:Eu^{3+} had lowest luminescence intensity. This was considered due to possibility for Eu^{3+} (1.08 Å) ions to substitute Y^{3+} (1.04˚A) was more due to similarity in the ionic radii. While in case of Mg^{2+} (0.86 Å), chances for the substitution were less due to small ionic radius. Also, the substitution of Mg^{2+}/Eu^{3+} was less likely to happen energetically because of different valence states. It was further observed that on increasing calcination temperature, the luminescence intensity of these materials enhanced.

Lojpur et al. [39] studied the temperature dependence emission spectra of Eu^{3+}-doped SrY_2O_4 from 20 to 200 °C synthesized via sol–gel method. It was found that increase in temperature resulted in emission quenching. In the range from 20 to 200 °C, emission intensity was reduced by a factor of two. Two distinct emission peaks at 580.8 and 582.1 nm confirmed the two distinctive crystallographic environments for Eu^{3+} ions in the host lattice. This supported the assumption of two different Y^{3+} sites in the system. Also, the more intense emission at 611 nm than at 616.5 nm indicated the favored occupancy of Eu^{3+} at Y1 site. The emission intensity rapidly increased with concentration until the concentration of 3% and then decreased between 3 and 5%.

3.1.2 SYO:Tb phosphors

Pavitra et al. [27] studied the luminescent properties of SYO:Tb^{3+} phosphors synthesized via sol–gel method. The PLE spectra on monitoring at 543 nm of SYO:Tb^{3+} consisted of broadband from 220 to 350 nm with band maximum at 293 nm due to f–d transition of Tb^{3+}. It was observed that peaks moved towards the lower energy side with increasing Tb^{3+} concentration due to the increased crystal field splitting with increasing Tb^{3+} concentration. The crystal field splitting was increased due to the shortening of the distance between the central metal (Y) ion and its ligands (O). The PL emission spectra at 296 nm for different Tb^{3+} concentrations consisted of peaks typical of Tb^{3+} ions. The first group of emission bands associated with the transition $^5D_3$–$^7F_{J\ (J=5,4,\text{ and }3)}$ were found at 419, 437, and 459 nm. Whereas the second group of emission bands were placed at 485, 543, 586, and 623 nm belonging to the $^5D_4$–$^7F_{J(J=6,5,4\text{ and }3)}$ transitions. An intense green color was observed due to the magnetic dipole transition $^5D_4$–$^7F_5$ at 543 nm. At higher Tb^{3+} concentration, the blue emission peaks were suppressed due to the cross-relaxation effect. The PL intensity decreased with increasing Tb^{3+} concentration at above 1 mol% due to concentration quenching.

In continuation of their study, Pavitra et al. [27] studied the effect of Eu^{3+} co-doping in SYO:Tb^{3+} phosphors. The deconvoluted excitation spectra of $SrY_{2(1-(x+y))}O_4$: $2x$$Tb^{3+}$/$2y$$Eu^{3+}$ (x and $y = 0.5$ and 1 mol%) at emission wavelengths of 616 nm (Eu^{3+}) and 543 nm (Tb^{3+}) consisted of peak centerd at 254 nm due to the CTB of Eu^{3+} ions and peak centered at 275 nm due to the spin-allowed transition between $^7F_6$ ground state and $^7D_{J(=5,4,3,2,1)}$ multiplets. The other peak centered around 294 nm was due to spin-forbidden transition between the $^7F^6$ ground state and $^9D_{J(=6,5,4,3)}$ multiplets of the Tb^{3+} ion. It was found that the excitation intensity of Eu^{3+} ions increased with increasing Eu^{3+} concentration at the rate of Tb^{3+} energy, which confirmed the efficient energy transfer from Tb^{3+} to Eu^{3+} ions. The energy transfer from Tb^{3+} to Eu^{3+} occurred due to the cross-relaxation process. When excited with 275 or 296 nm, the energy transfer to the $^5F_3$ excitation levels of the Eu^{3+} ion took place and then it transferred non-radiatively to the $^5D_0$ metastable state. On the other hand, as the emissions bands were overlapped well with the absorption bands which led to energy transfer occurred through the cross-relaxation process. It was found that adjusting the Tb and Eu concentration; white illumination was achieved. The CIE coordinates for 0.5 Tb^{3+}/0.5 Eu^{3+}, 0.5 Tb^{3+}/1 Eu^{3+}, 1 Tb^{3+}/0.5 Eu^{3+}, and 1 Tb^{3+}/1 Eu^{3+} were calculated to be (0.406, 0.417), (0.407, 0.402), (0.391, 0.406), and (0.401, 0.413), respectively. It was also found that for excitation wavelength at 281 nm, 0.5, and 1 mol% Eu^{3+}

ions co-doped with 0.5 mol% Tb^{3+}:SYO sample, the Eu^{3+} emission intensity was very high compared to Tb^{3+} emission intensity due to the high energy transfer efficiency.

Further, Pavitra et al. [27] studied the energy transfer mechanism in Sm^{3+} co-doped SYO:Tb^{3+} phosphor. It was observed that excitation spectra of Tb^{3+}- and Tb^{3+}/Sm^{3+}-doped SY phosphors at 543 nm (Tb^{3+}) exhibited similar excitation peaks with a strong broadband due to $^4F_7$–$^5D_1$ centered at 296 nm. Whereas the excitation spectra of Tb^{3+}/Sm^{3+} activated SrY_2O_4 phosphors at 606 nm (Sm^{3+}) revealed weak HAB of Sm^{3+}, f–d transition of Tb^{3+} in the high energy region and strong f–f transitions in the lower energy region. It was observed that the emission band edge of Tb^{3+} overlapped with Sm^{3+} emission ($^4G_{5/2}$–$^6H_{7/2}$) when excited with 606 nm. It was found that all excitation spectra of SYO at different emission wavelengths showed a common excitation band at 380 nm due to $^7F_6$–$^5D_2$ of Tb^{3+}, and $^6H_{5/2}$–$^4K_{13/2}$ of Sm^{3+}. The emission spectra consisted of blue and green emission bands of Tb^{3+} ions including weak Sm^{3+} transitions upon excitation at 296 nm wavelengths. The CIE chromaticity coordinates changed from (0.315, 0.505) to (0.328, 0.451), under different excitation wavelengths. The emission spectra at 380 nm wavelengths covered the total visible spectra due to the presence of both Tb^{3+} and Sm^{3+} emission lines, resulting in white emission. It was observed that blue emission lines showed some reasonable intensity in case of SYO:Tb,Eu as compared to SYO:Tb. This indicated the efficient energy transfer from Tb^{3+} to Sm^{3+}. The white light emission was also observed by adjusting the Sm^{3+} and Tb^{3+} concentrations and excitation wavelength.

Taikar [18] studied singly doped SrY_2O_4 phosphors activated with Tb^{3+}. The excitation spectrum exhibited transitions related to f orbital of Tb^{3+}. The emission spectra of SrY_2O_4:Tb^{3+} showed both blue and green emissions due to transitions from $^5D_3$–^7F_j and $^5D_4$–^7F_j state. The CIE coordinates for SrY_2O_4:Tb^{3+} were found to be (0.211, 0.518) with color purity of 62.54%. Zhang et al. [17] explained that the emission intensity of $^5D_3$ decreased with increasing Tb^{3+} concentration, accompanied by the enhancement of the emission from the $^5D_4$ level due to the cross-relaxation via the resonant energy transfer process: Tb^{3+} ($^5D_3$) + Tb^{3+} ($^7F_6$) → Tb^{3+} ($^5D_4$) + Tb^{3+} ($^7F_0$). In order to support the cross-relaxation phenomena, the critical distance between Tb–Tb ions was calculated. This was because the energy transfer results from the exchange interaction, the critical distance between the sensitizer and activator should be shorter than 4 Å. However, in their study, the critical distance was found to be 21.38 Å, which was much higher than 4 Å, indicating little possibility of cross-relaxation via the exchange interaction mechanism. This led to the conclusion that cross-relaxation between the Tb^{3+} ions mainly took place via electric dipole–dipole interactions.

3.1.3 SYO:Sm phosphors

Pavitra et al. [27] studied the luminescent characteristics of Sm-doped SYO phosphors synthesized via sol–gel method. The PLE spectra consisted of series of peaks of Sm^{3+} annealed at 1300 °C when monitored at emission wavelength at 608 nm. The PLE spectra showed a weak host absorption band (HAB) in the shorter and longer wavelength regions. The Sm^{3+} activated SYO emission under a UV lamp (at 408 nm) exhibited a considerable similarity in the emission color of Sm^{3+} and Eu^{3+} in SrY_2O_4 host lattice. The emission spectra of Sm^{3+} showed reasonable emission at 566 nm due to $^4G_{5/2}$–$^6H_{5/2}$ transition, strong, and efficient emission at 606 nm due to $^4G_{5/2}$–$^6H_{7/2}$ transition, and weak emission at 658 nm due to $^4G_{5/2}$–$^6H_{9/2}$ transition. Taikar [18] studied singly doped SrY_2O_4 phosphors activated with Sm^{3+} synthesized via combustion method. The excitation spectrum gave good overlap in near-UV region and hence on excitation showed orange emission (excited at 409 nm) having high quantum efficiency (75.3%). The CIE coordinates for SrY_2O_4: Sm^{3+} were found to be (0.575, 0.425).

3.1.4 SYO:Dy phosphors

Zhang et al. [17] showed that the emission ratio (Y/B) of Dy^{3+} could be used as a probe to detect the local symmetry of the activator ions as Dy^{3+} (Y^{3+}) ions have two non-equivalent sites and six oxygen atoms coordinate both sites with C_s symmetry exhibiting an asymmetrical chemical environment. Therefore, the yellow emission dominated the blue emission in the emission spectra. The maximum PL was found for 0.005 and 0.007 concentrations of Tm and Dy ions, respectively, which are of very small concentration values. This was because of short Y–Y bond distance due to the double octahedral of $Y_2O_4^{2-}$ in SrY_2O_4 compound. It was observed that the concentration quenching of Dy^{3+} was mainly caused by cross relaxation, i.e., energy transfer among Dy^{3+} ions via Dy^{3+} ($^4F_{9/2}$) + Dy^{3+} ($^6H_{15/2}$) → Dy^{3+} ($^6F_{3/2}$) + Dy^{3+} ($^6F_{11/2}$) mechanism.

Pavitra et al. [15] also studied the photoluminescence in Dy^{3+}-doped SrY_2O_4 phosphors synthesized via citrate sol–gel method. The PL spectra at 578 nm emission, consisted of the charge-transfer state (CTS) between 257 and 307 nm and f–f transitions at 325 nm ($^6H_{15/2}$–$^6P_{3/2}$), 351 nm ($^6H_{15/2}$–$^6P_{7/2}$), 365 nm ($^6H_{15/2}$–$^6P_{5/2}$), 387 nm ($^6H_{15/2}$–$^4I_{13/2}$), 426 nm ($^6H_{15/2}$–$^4G_{11/2}$), and at 451 nm ($^6H_{15/2}$–$^4I_{15/2}$). The emission studies of the phosphors at 351 nm excitation revealed three typical peaks at 488 nm (blue) ($^4F_{9/2}$–$^6H_{15/2}$), 578 nm (yellow) ($^4F_{9/2}$–$^6H_{13/2}$) and 678 nm (red) ($^4F_{9/2}$–$^6H_{11/2}$) of Dy^{3+} ions. It was reported that Dy-activated SYO nanocrystalline phosphors emitted cool white light. The domination of yellow band over the blue band signified that Dy^{3+} ions occupied the low symmetry sites.

The optimum concentration was found at 1 mol%. Pavitra et al. [15] monitored the luminescent characteristics of SrY_2O_4:1Dy^{3+}/1Eu^{3+} nanocrystalline phosphors. The excitation spectra monitored at 578 nm ($^4F_{9/2}$–$^6H_{13/2}$) and 615 nm ($^5D_0$–$^7F_2$) consisted of broad excitation band with band maxima at 271 nm in the shorter wavelength region, and some sharp excitation peaks in the longer wavelength region due to the f–f transitions of Dy^{3+} and Eu^{3+} ions. It was observed that the intensity of excitation peaks were high when monitored under 578 nm as compared to 615 nm. The deconvoluted broad excitation band of the SrY_2O_4:1Dy^{3+}/1Eu^{3+} co-activated nanocrystalline phosphor showed three bands using Gaussian fitting. The band centered at 232 nm was HAB and this band occurred due to Dy^{3+} ions. The remaining two bands with band maxima located at 264 and 275 nm were the CTBs of Eu^{3+} ions due to the presence of two Y sites in the SrY_2O_4 host lattice. The PL emission spectra of SrY_2O_4:Dy^{3+}/Eu^{3+} nanocrystalline phosphor were studied as a function of Eu^{3+} ion concentration for a fixed 1 mol% of Dy^{3+} ion by exciting at 381 nm. The PL emission spectra showed various emission peaks originating from $^5D_{J(J=0,1,2,3)}$ levels of Eu^{3+} ions. It was observed that blue and yellow emission bands of Dy^{3+} ions were split into doublets. The blue emission band splitted into two peaks occurring at 466 and 490 nm, and the yellow emission band was split into two intense peaks occurring at 578 and 590 nm. With the increase in the Eu^{3+} ion concentration (i.e., 1:2, 1:3 ratios), the emission peak intensity corresponding to the hypersensitive electric dipole transition ($^5D_0$–$^7F_2$) of Eu^{3+} ions at 614 nm exhibited a systematic enhancement due to the energy transfer from Dy^{3+} to Eu^{3+} ions.

3.1.5 SYO:Er phosphors

Pavitra et al. [16] prepared SrY_2O_4:Er^{3+} nanocrystalline phosphors using citrate sol–gel process. PL excitation (PLE) spectra of SrY_2O_4:Er^{3+} nanocrystalline phosphors at emission wavelength of 548 nm ($^4S_{3/2}$–$^4I_{15/2}$), consisted of intra 4f transitions of Er^{3+} ions in the longer wavelength region. Upon excitation at 378 nm ($^4I_{15/2}$–$^4G_{11/2}$), the emission spectra consisted of peaks at 525 ($^2H_{11/2}$–$^4I_{15/2}$) and 548 nm ($^4S_{3/2}$–$^4I_{15/2}$). A small feeble peak at 660 nm ($^4F_{9/2}$–$^4I_{15/2}$) was also observed. The optimum concentration of Er^{3+} ions was 1 mol% and then concentration quenching occurred. The CIE chromaticity coordinates for the prepared phosphors lie in the green region.

In another study, Pavitra et al. [16] prepared the Dy^{3+}/Er^{3+} ions co-doped SYO phosphors showing yellowish green emissions. The PLE spectra of SrY_2O_4:1 mol%Dy^{3+}/1 mol% Er^{3+} nanocrystalline phosphors at 548 ($^4S_{3/2}$–$^4I_{15/2}$) and 578 nm ($^4F_{9/2}$–$^6H_{13/2}$) were monitored. It was found that when the SrY_2O_4:1Dy^{3+}/1Er^{3+} were excited at 548 nm, the spectrum consisted of only sharp excitation peaks in the longer wavelength region corresponding to the f–f transitions of Er^{3+} ions. Similarly, when SrY_2O_4:1Dy^{3+}/1Er^{3+} sample was excited at 578 nm, the spectrum involved HAB in the shorter wavelength region. This was attributed to the efficient energy transfer from the host to the Dy^{3+} ions. Also, some sharp excitation peaks due to f–f electronic transitions for Dy^{3+} ions were also observed. In both spectra, a common excitation peak was observed at 365 nm due to electronic transitions of Dy^{3+} ions ($^6H_{15/2}$–$^6P_{5/2}$) and Er^{3+} ions ($^4I_{15/2}$–$^4G_{9/2}$). Thus, it was observed that co-doped sample can be efficiently excited by near-UV excitation at 365 nm. The PL emission spectra of SrY_2O_4:Dy^{3+}/Er^{3+} consisted of two intense emission bands in the blue and yellow regions at 489 nm and 578 nm and one weak emission band in the red region at 678 nm due to Dy^{3+} ions. Similarly, the Er^{3+} ions gave two intense emission bands in the green region and one weak band in the red region. By increasing the Er^{3+} ion concentration, it was found that the emission peak intensity corresponding to the ($^4S_{3/2}$–$^4I_{15/2}$) transition increased due to the improved energy transfer from Dy^{3+} to Er^{3+} ions. The energy transfer efficiencies for the co-doped samples by varying the Er^{3+} concentration and keeping Dy^{3+} concentration constant were calculated to be 13.34, 22.09, and 34.76% for 1Dy^{3+}/1Er^{3+}, 1Dy^{3+}/1.5Er^{3+}, and Dy^{3+}/2Er^{3+}, respectively. The CIE chromaticity coordinates for the co-doped samples lie in fair white light region.

3.1.6 SYO:Ce phosphors

Blasse and Bril 1967 [42] studied SrY_2O_4-Ce phosphors prepared by firing intimate mixtures of high-purity oxides at appropriate temperatures in nitrogen. The fluorescence emission in the case of oxidic host lattices had peaks in the near UV due to the exceptionally large stokes shift of the emission. It was reported that such a large Stokes shift was observed due to the difference between the equilibrium distance of the excited state and that of the ground state was high. For SrY_2O_4–Ce, it was observed that the light output at 200 K was only 20% as that at l00 K. In another study, Manivannan et al. [43] prepared Ce–SrY_2O_4 by conventional ceramic method in the hydrogen environment. The samples showed blue and green emission band typical of Ce^{3+} 5d–4f transitions. It was interesting to note that blue emission band was absent in the air synthesized samples. Also, the decay time of blue band as a function of temperature was single exponential with a decay constant of about 37 ns and was independent of temperature between 10 and 300 K. These observations strongly pointed to the trivalent cerium as being responsible for the blue emission band. The green emission was also observed which was attributed to the presence of Ce^{4+}–O^{2-} charge-transfer transition in Sr_2CeO_4. It was further found that the decay time of the charge-transfer state in Sr_2CeO_4 was long (65 ms). With an

increase in temperature from 5 to 25 K, the emission intensity increased, beyond which it decreased. Similar results of emission spectra of SrY_2O_4:Ce^{3+} phosphors were reported by Philippen et al. [40].

Taikar [18] studied the luminescent properties of Ce^{3+}-doped SrY_2O_4 phosphors synthesized via combustion method. The excitation spectra of SrY_2O_4:Ce^{3+} exhibited broad band at 345 nm which was attributed to transitions from ground state of $^4f_1$ configuration to states of $^5d_1$ configuration of typical Ce^{3+} ion. Under 345 nm excitation, emission spectra consisted of broadband extending from 390 to 590 nm with a peak at around 460 nm and shoulder around 505 nm. The emission peaks were attributed to the transition from the 5d level to the ground state ($^2F_{5/2}$–$^2F_{7/2}$) of the Ce^{3+} ions. The Gaussian deconvolution of the emission band gave two well-separated Gaussian components with maxima at 460 nm (21,739 cm^{-1}) and 505 nm (19,801 cm^{-1}). It was found that Gaussian component curve on an energy scale was in good agreement with the theoretical difference between the $^2F_{5/2}$ and $^2F_{7/2}$ levels (about 2000 cm^{-1}). The color coordinates for Ce^{3+}-doped SrY_2O_4 phosphor were found to be (0.1526, 0.2069).

3.1.7 SYO:Bi phosphors

Taikar [18] studied the luminescent properties of Bi^{3+}-doped SrY_2O_4 phosphors. The excitation spectrum of SrY_2O_4:Bi^{3+} consisted of small peak around 240 and highly intense excitation peak at 330 nm. The 330 nm peak was attributed to $^1S_0$–$^3P_1$ transition of Bi^{3+} ion. At 330 nm excitation, PL emission spectra consisted of broadband ranging from 350 to 530 nm with peak maxima around 420 nm. The emission band was attributed to $^3P_1$, $^3P_0$–$^1S_0$ transition of Bi^{3+} ion. The color coordinate for Bi^{3+}-doped SrY_2O_4 phosphor were found to be (0.1582, 0.035).

Wei et al. [22] studied the energy transfer mechanism in SrY_2O_4:Bi^{3+},Eu^{3+} (SYO:Bi^{3+},Eu^{3+}) phosphors. Firstly, the concentration of Bi ions was varied in the host lattice. The excitation spectra consisted peak of 330 nm ($^1S_0$–$^3P_1$ transition of Bi^{3+}) when monitored at 410 nm. Then, under excitation at 330 nm, the emission spectra consisted of emission peak at 410 nm originating from $^3P_1$–$^1S_0$ transition of Bi^{3+} ions. The maximum PL was found for 0.024 of Bi ions. To this optimized sample (SYO:0.024Bi^{3+}), Eu ions were co-doped and the maximum intensity was found for 0.32 of Eu ions. Under excitation at 330 nm, the emission spectra of SYO:Bi, Eu phosphors consisted of emission peaks in the blue and as well as in red region ranging from 550 to 720 nm. It was noted that the energy transfer efficiency from Bi^{3+} to Eu^{3+} was found to be 92.65%. A tunable emission was achieved from blue (0.179, 0.266) to red (0.620, 0.339) in SYO:Bi^{3+},Eu^{3+} by changing the concentration of Bi^{3+} and Eu^{3+}. It was also observed that emission intensity of the phosphors at 155 °C was maintained over 98% emission intensity of that at 35 °C. In continuation of their earlier studies, Wei et al. [34] also studied the temperature-dependent emission behaviors of SYO:0.024Bi^{3+}, 0.09Eu^{3+} under excitation at 330 nm. It was observed that Bi^{3+} and Eu^{3+} showed significantly different temperature-dependent emission behaviors. The luminescent intensity of Bi^{3+} increased, whereas Eu^{3+} weakened gradually when temperature was increased from 313 to 563 K. The CIE color coordinates changed from (0.4268, 0.2270) to (0.2281, 0.1157) with enhancing temperature from 313 to 563 K.

3.2 Upconversion in SYO phosphors

3.2.1 SYO:Er phosphor

Mukhopadhyay et al. [44] studied the upconversion luminescent properties of Er-doped SrY_2O_4 phosphors synthesized via chemical co-precipitation method. Under laser excitation at 980 nm, the emission spectra consisted of peaks at 490 nm, 525 nm, 550 nm, 667 nm, and 798 nm corresponding to the $^4F_{7/2}$–$^4I_{15/2}$, $^2H_{11/2}$–$^4I_{15/2}$, $^4S_{3/2}$–$^4I_{15/2}$, $^4F_{9/2}$–$^4I_{15/2}$ and $^4I_{9/2}$–$^4I_{15/2}$ transitions of Er^{3+} ions, respectively. The maximum PL was obtained for 5 mol% of Er ions. It was found that two photons accompanied the UC process. The CIE coordinates of the SYO:Er phosphors were found to be (0.23, 0.73), lying in the pure green region.

3.2.2 SYO:Er, Yb phosphors

Shen et al. [33] studied the luminescent properties of SrY_2O_4:Er, Yb under 1550 and 980 nm laser excitations. The UC emission spectra under excitation at 1550 nm consisted of peaks in the regions of 510–542 nm, 543–570 nm, and 634–681 nm, of Er^{3+} ions, respectively. The different transitions and energy transfer involved in SYO:Er, Yb under 1550 nm excitation are shown in Fig. 4. Similar results for the UC spectra at 980 nm excitation were found but different relative intensities. The emission studies showed that maximum red and green emission intensity under excitation at 980 and 1550 nm was found for SrY_2O_4:0.12Er, 0.01Yb sample. The red to green emission intensity ratio varied as a function of pumping current, at 980 and 1550 nm excitation. It was observed that the said ratio increased with increasing Yb^{3+} ion concentration but decreased as the excitation power increased under 980 nm and 1550 nm pumping. The change in red to green emission intensity ratio was also higher at 1550 nm excitation than at 980 nm excitation.

3.2.3 Tri-doping in SYO

In another study, Pavitra et al. [16] studied the luminescent features with tri-doping of Er^{3+}/Dy^{3+}/Sm^{3+} ions in SrY_2O_4

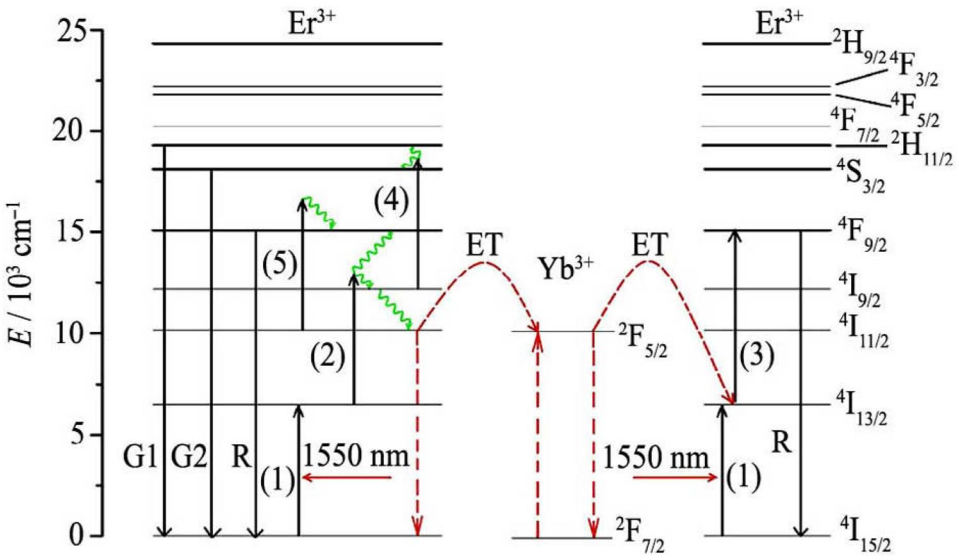

Fig. 4 Schematic diagram of SYO:0.12Er,0.01Yb/SYO:0.12Er,0.08Yb energy levels [33] (with permission)

host lattice. The PLE spectra of $1Dy^{3+}/1Er^{3+}/1Sm^{3+}$ triple-doped SrY_2O_4 nanocrystalline phosphors at different emission wavelengths of 578 nm (Dy^{3+}), 561 nm (Er^{3+}), 548 nm (Er^{3+}), and 606 nm (Sm^{3+}) exhibited host absorption band in shorter wavelength region along with respective sharp excitation bands due to f–f transitions of Dy^{3+}, Er^{3+}, and Sm^{3+} ions in the longer wavelength region. It was found that a common excitation peak around 365 nm was observed in all PLE spectra, so 365 nm was used as an excitation wavelength. The PL emission spectra of $1Dy^{3+}/1Er^{3+}/xSm^{3+}$ ($x = 0.25$, 0.5, 1, and 2 mol%) ions triple-doped SrY_2O_4 nanocrystalline phosphors as a function of Sm^{3+} ion concentration under excitation at 365 nm exhibited all three RE ions (Dy^{3+}, Er^{3+}, and Sm^{3+}) emission bands, suggesting that the availability of triple co-doped ions in the host lattice. The PL intensity increased with increased concentration of Sm ions. The emission peak intensity corresponding to the ($^4G_{5/2}$–$^6H_{7/2}$) transition of Sm^{3+} ions was increased, which was attributed to the energy transfer from $^4F_{9/2}$ energy levels of Dy^{3+} ion and $^4F_{7/2}$ level of Er^{3+} to $^4G_{5/2}$ level of Sm^{3+} ions. The energy transfer efficiencies for $1Dy^{3+}/1Er^{3+}/0.25Sm^{3+}$, $1Dy^{3+}/1Er^{3+}/0.5Sm^{3+}$, $1Dy^{3+}/1Er^{3+}/1Sm^{3+}$, and $1Dy^{3+}/1Er^{3+}/2Sm^{3+}$ were calculated to be 14.37, 33.68, 63.49, and 69.32%, respectively. PL analysis showed that the triple-doped SrY_2O_4 phosphors exhibited a fair white light emission and the CIE chromaticity coordinates were lying in warm-white light region.

Further, Pavitra et al. [45] studied the luminescent properties of tri-doped (Er, Tm, Tb) SrY_2O_4 nanocrystalline phosphors. The UC emission spectra consisted of blue emission band at 487 nm due to Tm^{3+} ions, green emission bands at 526 nm and 551 nm due to Er^{3+} ions and red emission band at 664 nm due to the Er^{3+} and Tm^{3+} ions, respectively. The various transitions and enrgy transfer mechanisms involved in the UC process of Er^{3+}, Tm^{3+} and Yb^{3+} tri-doped SYO are shown in Fig. 5. It was observed that when pump power was changed from 100 to 300 mW, the red emission band at 664 nm was dominant in the spectra. With further increase in pump power from 300 to 900 mW, the blue emission intensity increased gradually. This occurred due to possible energy transfer between the Er^{3+} and Tm^{3+} ions. When the $Er^{3+}/Tm^{3+}/Yb^{3+}$ ions were tri-doped, the $^4I_{11/2}$ level of the Er^{3+} ions and the $^3H_5$ level of the Tm^{3+} ions were populated by the energy transfer from the $^2F_{5/2}$ level of the Yb^{3+} ions, there was a chance for an energy transfer from the $^4I_{11/2}$ (Er^{3+}) level to the $^3H_5$ (Tm^{3+}) level by phonon assistance.

4 Outlook and summary

In conclusion, it is observed that SYO is a promising host lattice for doping different rare and non-rare earth elements. The chemical and thermal stability makes it a prestigious host lattice in the family of AB_2O_4 oxides. SYO is synthesized via different routes such as solid-state, sol–gel, combustion, microemulsion and aldo–keto methods. Out of these, citrate sol–gel method is found to be effective than other methods. The SYO phosphors obtained by this method are monodisperse, less aggregated and having close-packed structures. SYO on doping with different elements give different emission spectra under different excitation wavelengths in UV and vacuum UV excitation. In addition to this, SYO phosphors are more appealing due to their high water-resistant and unique luminescence characteristics. However, there are challenges in the synthesis of SYO. The methods as mentioned above, are either high temperature routes or proceed via complicated routes. It is also observed that the synthesized materials

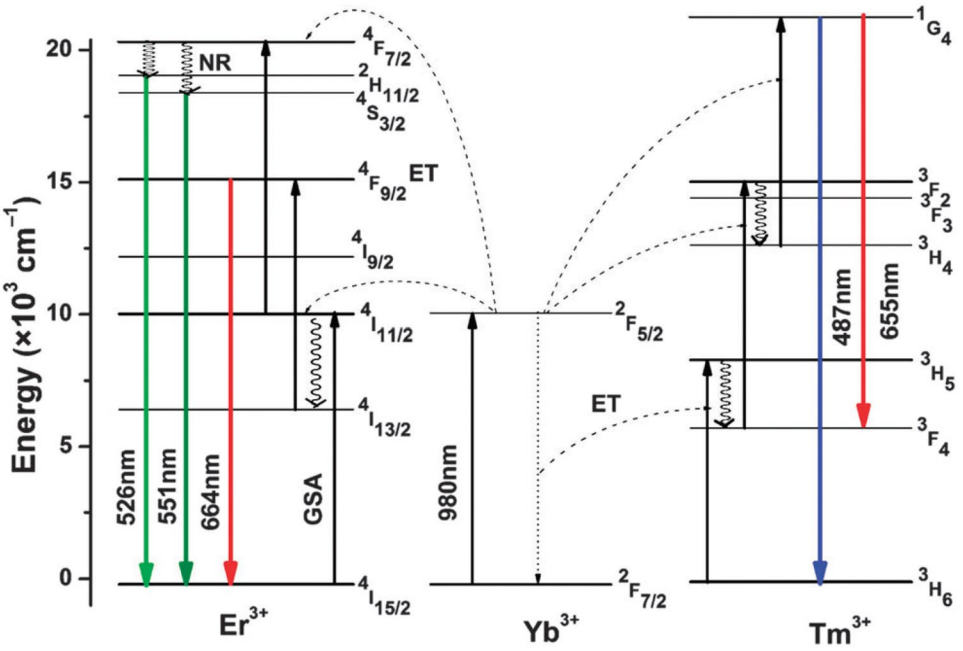

Fig. 5 Energy level diagram of Er^{3+}, Tm^{3+} and Yb^{3+} tri-doped SYO nanocrystalline phosphors [45] (with permission)

have impurities of SrO and Y_2O_3 upto some extent. The synthesized phosphors are generally microcrystalline in nature and agglomerated. So, it is necessary to find the effective synthesis routes to synthesize nanocrystalline, monodisperse and phase pure SYO phosphors. The use of surfactants can be done to avoid the agglomeration and synthesis of particles in the nanoregime. Moreover, the morphology can be engineered to alter the luminescent properties. The crystal structure of SYO needs to be refined by some refinement tools to study the effective occupancy of ions at sites. To the best of our knowledge, there are very few studies reported in this context. From PL results, it is observed that there are different sites in the SYO lattice. However, the percentage occupancy of different sites and their relation with luminescent behavior are not studied. Also, the local environment of the activators in SYO crystal field is not studied on theoretical grounds. The photometric parameters such as CIE coordinates, CCT, CRI, decay curves, quantam yield, and activation energies can be studied in detail. The reports which deal with the SYO are generally related to the doping of the rare earth elements. However, doping with non-rare earth elements such as Mn^{2+}/Mn^{4+}, Cr^{3+}, and Cu^{2+} are not studied. In addition to this, co-doping with non-rare earth elements such as alkali and alkaline earth metals can be done to improve the luminescent characteristics further.

Compliance with ethical standards

Conflicts of interest The authors claim no conflicts of interest.

References

1. N. Hirosaki, R. Xie, K. Inoue, T. Sekiguchi, B. Dierre, Appl. Phys. Lett. **2**, 061101 (2007)
2. G. Li, X. Xu, C. Peng, M. Shang, D. Geng, J. Chen, J. Lin, Fluoresc. Lumin. Mater. **19**, 3020 (2011)
3. C.S. Kamal, T.K.V. Rao, T. Samuel, P.V.S.S.S.N. Reddy, J.B. Jasinski, Y. Ramakrishna, M.C. Rao, K.R. Rao, RSC Adv. **7**, 44915 (2017)
4. A.A. Talin, K.A. Dean, J.E. Jaskie, Solid State Electron. **45**, 963 (2001)
5. P.H. Holloway, T.A. Trottier, B. Abrams, C. Kondoleon, S.L. Jones, J.S. Sebastian, W.J. Thomest, J. Vac. Sci. Technol. B **17**, 758 (1999)
6. A. Manohar, C. Krishnamoorthi, J. Alloys Compd. **722**, 818–827 (2017)
7. J. Singh, J. Manam, Ceram. Int. **44**, 10912–10920 (2016)
8. R.W. Grimes, A.B. Anderson, A.H. Heuerg, J. Am. Soc. **111**, 1 (1989)
9. J. Choisnet, M. Hervieu, B. Raveau, P. Tarte, J. Solid State Chem. **45**, 280 (1982)
10. K. Kurosaki, T. Tanaka, T. Maekawa, S. Yamanaka, J. Alloys Compd. **395**, 318 (2005)
11. K. Kurosaki, T. Tanaka, T. Maekawa, S. Yamanaka, J. Alloys Compd. **398**, 304 (2005)
12. S.-J. Park, C.-H. Park, Yu Byung-Yong, H.-S. Bae, C.-H. Kim, C.-H. Pyun, J. Electrochem. Soc. **146**, 3903 (1999)
13. S.P. Ghorpade, N.R.P. De, R. Soc. Chem. **10**, 21049 (2020)
14. V. Dubey, J. Kaur, S. Agrawal, N.S. Suryanarayana, K.V.R. Murthy, Optik (Stuttg) **124**, 5585 (2013)
15. E. Pavitra, G. Seeta Rama Raju, W. Park, J.S. Yu, New J. Chem. **38**, 163 (2014)
16. E. Pavitra, G.S.R. Raju, J.S. Yu, J. Alloys Compd. **592**, 157 (2014)
17. Y. Zhang, D. Geng, M. Shang, X. Zhang, X. Li, Z. Cheng, H. Lian, J. Lin, Daltan Trans. **42**, 4799 (2013)
18. D.R. Taikar, J. Lumin. **204**, 24 (2018)
19. C.M. Mehare, Y.R. Parauha, N.S. Dhoble, S.J. Dhoble, J. Mol. Struct. **2**, 127957 (2020)

20. D. Wang, Y. Wang, L. Wang, J. Lumin. **126**, 135 (2007)
21. V. Lojpur, S. Stojadinović, M. Mitrić, Sci. Sinter. **50**, 347 (2018)
22. R. Wei, Z. Zheng, Y. Shi, X. Peng, H. Wang, X. Tian, F. Hu, H. Guo, J. Alloys Compd. **767**, 403 (2018)
23. Z. Fu, S. Zhou, S. Zhang, J. Opt. Soc. Am. B **23**, 1852 (2006)
24. R. Atkins, A.L. Diaz, J. Lumin. **128**, 1463 (2008)
25. D. Singh, V. Tanwar, S. Bhagwan, V. Nishal, S. Sheoran, S. Kadyan, A.P. Samantilleke, P.S. Kadyan, Indian J. Mater. Sci. **2015**, 1 (2015)
26. R.K. Tamrakar, K. Upadhyay, J. Electron. Mater. **47**, 651 (2018)
27. E. Pavitra, G.S.R. Raju, Y.H. Ko, J.S. Yu, Phys. Chem. Chem. Phys. **14**, 11296 (2012)
28. J. Zhang, Y. Wang, J. Mater. Res. **25**, 2120 (2010)
29. V. Singh, K. Swapna, S. Kaur, A.S. Rao, J.L. Rao, J. Electron. Mater. **5**, 11296 (2020)
30. W. Xu, W. Jia, I. Revira, K. Monge, H. Liu, J. Electrochem. Soc. **148**, H176 (2001)
31. Z. Fu, S. Zhou, Y. Yu, S. Zhang, J. Phys. Chem. B **109**, 23320 (2006)
32. T. Opravil, P. Ptáček, F. Šoukal, E. Bartoníčková, J. Wasserbauer, J. Therm. Anal. Calorim. **123**, 181 (2016)
33. X. Shen, M. Xing, Y. Tian, Y. Fu, Y. Peng, X. Luo, J. Rare Earths **34**, 458 (2016)
34. R. Wei, J. Guo, K. Li, L. Yang, X. Tian, X. Li, F. Hu, H. Guo, J. Lumin. **216**, 116737 (2019)
35. K.A. Koparkar, N.S. Bajaj, S.K. Omanwar, Int. J. Lumin. Appl. **5**, 134 (2015)
36. L. Zhou, J. Shi, M. Gong, Mater. Lett. **59**, 2079 (2005)
37. S.P. Ghorpade, R.H. Krishna, R.M. Melavanki, V. Dubey, Opt. Int. J. Light Electron Opt. **208**, 164533 (2020)
38. L. Zhou, J. Shi, M. Gong, J. Lumin. **113**, 285 (2005)
39. V. Lojpur, Z. Antic, M.D. Dramicanin, R. Soc. Chem. **35**(15), 4428–4435 (2014)
40. J. Philippen, C. Guguschev, D. Klimm-Leibniz, J. Cryst. Growth **459**, 17 (2018)
41. E.B. Shaik, S. Rajyalakshmi, M.S.S. Dharmaja, B.V. Sangeetha, R.S. Lakshmi, Y.R. Krishna, K.R. Rao, AIP Conf. Proc. **1992**, 3 (2018)
42. G. Blasse, A. Bril, J. Chem. Phys. **47**, 5139 (1967)
43. V. Manivannan, H.A. Comanzo, A.A. Setlur, A.M. Srivastava, J. Lumin. **103**, 635 (2003)
44. L. Mukhopadhyay, V. K. Rai, in *2018 3rd Int. Conf. Microw. Photonics* (ICMAP 2018), 9–11 February (2018).
45. E. Pavitra, G. Seeta-Rama-Raju, J.-H. Oh, J.S. Yu, R. Soc. Chem. **38**, 3413 (2014)